JOURNAL OF MAGNETIC RESONANCE **135,** 169–177 (1998)
ARTICLE NO. MN981573

Determination of the Peptide Torsion Angle ϕ by ^{15}N Chemical Shift and $^{13}C^{\alpha}$-$^{1}H^{\alpha}$ Dipolar Tensor Correlation in Solid-State MAS NMR

M. Hong,*[,1] J. D. Gross,* W. Hu,† and R. G. Griffin*[,2]

*Francis Bitter Magnet Laboratory and Department of Chemistry, Massachusetts Institute of Technology, Cambridge, Massachusetts 02139; and †Department of Polymer Science and Engineering, University of Massachusetts, Amherst, Massachusetts 01003

Received February 11, 1998; revised July 31, 1998

We demonstrate a dipolar-chemical shift correlation technique for sign-sensitive determination of the torsion angle ϕ in solid peptides and proteins under magic-angle spinning. The indirect dimension of the experiment is obtained by separate but synchronous evolution of the magnetization under the ^{15}N chemical shift and the C-H dipolar coupling. The resulting sum and difference spectrum of the two frequencies, with more than ten independent sidebands, depends strongly on the relative orientation of the ^{15}N chemical shift tensor and the C^{α}-H^{α} bond. This relative orientation reflects the $C(O)_{i-1}$-N-C^{α}-$C(O)_i$ torsion angle. The technique can distinguish ϕ angles over the full range of 360° when the amide ^{15}N chemical shift tensor does not possess reflection symmetry with respect to the peptide plane. Thus it complements our previous HNCH experiment, in which two mirror-symmetric conformers of the H^N-N bond relative to the C^{α}-H^{α} bond around the N-C^{α} axis cannot be distinguished.

INTRODUCTION

The elucidation of the conformational structure of biological molecules such as polypeptides by nuclear magnetic resonance (NMR) spectroscopy has traditionally relied on the measurement of internuclear distances. Recently, however, several techniques were introduced which determine torsion angles by correlating two orientation-dependent interactions across the torsion axis of interest (*1–7*). By exploiting relatively strong spin interactions such as the chemical shift anisotropy or the dipolar coupling between directly bonded nuclei, the torsion angle techniques yield precise conformational information such as the secondary structure of polypeptides. Such information would be obtained with less precision by distance techniques, since they require measuring very weak dipolar couplings with high accuracy. For determining the peptide torsion angle ϕ in the $C(O)_{i-1}$-N-C^{α}-$C(O)_i$ segment, a 2D magic-angle spinning HNCH technique that we proposed recently seems particularly promising (*8, 9*). The ϕ torsion angle is extracted from the relative orientation of the N-H^N and C^{α}-H^{α} bonds, which is probed by evolving double- and zero-quantum (DQ/ZQ) N-C^{α} spin states under the N-H and C-H dipolar interactions. The torsion-angle dependent dipolar sideband spectra are manifested in the ω_1 dimension and are separated according to the C^{α} isotropic chemical shift in the ω_2 dimension. Thus, the technique is capable of simultaneously measuring torsion angles for spectrally resolved residues. In addition, it can be shown the technique has higher angular resolution in biologically relevant conformational regions than distance measuring techniques (*10*).

Using dipolar couplings as structural probes has the advantage that the unique axis of the dipolar tensor in the molecular segment is known, *a priori,* to be oriented along the internuclear vector. This makes it straightforward to convert the NMR spectral parameters into molecular parameters. However, the axial symmetry of the dipolar interactions and the symmetry of the dipolar spectra with respect to $\omega_1 = 0$ also have drawbacks. The latter reduces the number of independent sidebands by a factor of two, which represents a significant reduction of the information content of the spectra. The axial symmetry of the interactions makes it impossible to distinguish H^N-N-C^{α}-H^{α} conformations that are equidistant from the *trans* (H^N-N-C^{α}-H^{α} = 180°) or *cis* (H^N-N-C^{α}-H^{α} = 0°) configurations in opposite directions. Thus, H^N-N-C^{α}-H^{α} torsion angles with the same magnitude but opposite signs yield identical dipolar spectra. In terms of the ϕ torsion angle, this corresponds to a degeneracy for pairs of angles (ϕ, ϕ') that are symmetric with respect to −120° or 60°, i.e., $\phi + \phi' = -240°$. Since this inability to distinguish mirror symmetric conformations stems from the uniaxiality of the dipolar interaction, it is also found in the dipolar-coupling-based distance measuring techniques.

To determine torsion angles unambiguously, at least one non-uniaxial spin interaction is required in the correlation scheme. Further, the orientation of this non-uniaxial interaction tensor must be such that no principal axis is perpendicular to the torsional axis (*2*). In the case of the torsion angle ϕ, the anisotropic chemical shift of the backbone amide nitrogen is a suitable choice. The molecular orientation of the amide ^{15}N chemical shift tensor has been studied in several model peptides (*11–19*) and was found

[1] Current address: Department of Chemistry, University of Massachusetts, Amherst, MA 01003.

[2] To whom correspondence should be addressed: NW14-3220, Massachusetts Institute of Technology, 170 Albany St., Cambridge, MA 02139.

1090-7807/98 $25.00

to exhibit relatively small variations. The σ_{22} axis lies close to, but not necessarily along, the normal to the peptide plane. Among the experimental studies found, deviations from normality range from 0° to 20° in different peptides. The σ_{33} axis lies in the peptide plane and forms an angle of 135° to 140° with respect to the N-C^α bond. Once the ^{15}N tensor orientation is known, correlation of the ^{15}N chemical shift with an interaction at the C^α site should yield sign-specific information on the intervening torsion angle ϕ.

In this paper, we demonstrate the correlation of the ^{15}N chemical shift and the C^α-H^α dipolar coupling tensor orientations under magic-angle spinning (MAS) to determine the ϕ torsion angle. The technique resolves different residues by detecting the $^{13}C^\alpha$ isotropic chemical shift in the second dimension of the 2D experiment. To obtain MAS sideband patterns of the sum and difference of the ^{15}N chemical shift anisotropy (CSA) and the C^α-H^α dipolar coupling, separate but synchronous evolution under these two interactions (*9, 20*) is employed. Using the well-characterized model peptide N-acetyl-D, L-valine (NAV), we show that the technique exhibits the highest sensitivity to ϕ torsion angles in the β-sheet structure region. The requirements for a full determination of the ϕ torsion angle, including its sign, are discussed.

THEORY

In this section, we first describe the pulse sequence for correlating the backbone ^{15}N chemical shift interaction with the C^α-H^α dipolar coupling. We then show mathematically how the ϕ torsion angle affects the time and frequency signals of the indirect dimension of the 2D spectrum. Last, we present the simulated ^{15}N CSA/$C^\alpha H^\alpha$ spectra as a function of the ϕ angle.

Pulse sequence with synchronous ^{15}N CSA/^{13}C-^1H evolution. The radio frequency (RF) pulse sequence for the experiment is shown in Fig. 1. The main feature of the experiment is that the magnetization evolves rotor synchronously under the C-H dipolar coupling and the ^{15}N chemical shift interaction during two separately but synchronously incremented t_1 periods.

After cross polarization from ^1H to ^{13}C, antiphase magnetization C_xN_z is created by recoupling the N-C dipolar interaction with a REDOR sequence, which consists of alternating 180° pulses on ^{13}C and ^{15}N channels every half rotor cycle for two rotor periods (*21*). The magnetization evolves under the C-H dipolar interaction for a period defined by an MREV-8 multiple-pulse train, which attenuates the homonuclear ^1H-^1H coupling (*22*). The maximum MREV-8 duration or evolution time is one rotor period. The ^{13}C evolution period is part of a two-rotor-cycle constant time period that serves to refocus the ^{13}C chemical shift interaction and to maintain rotor phase coherence between the ^{13}C and the ^{15}N evolution periods. At the end of the constant time, the ^{13}C magnetization is transferred to ^{15}N spins by two simultaneous 90° pulses on the ^{13}C and ^{15}N channels. The resulting N_xC_z magnetization evolves

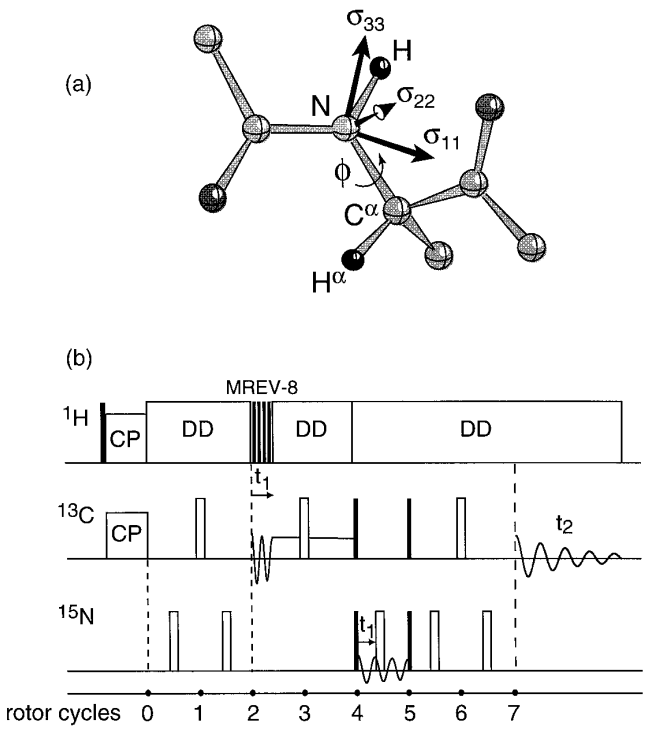

FIG. 1. Pulse sequence for measuring the ϕ torsion angle by correlating ^{15}N CSA and C^α-H^α dipolar coupling under MAS. The N-C^α dipolar coupling is recoupled with a REDOR sequence. During the t_1 period antiphase magnetization terms C_xN_z and C_zN_x evolve under the C-H dipolar coupling and the doubled ^{15}N CSA interaction separately but synchronously. The isotropic ^{13}C chemical shifts are detected during t_2 to provide site resolution. The phase cycles are identical to those used in Ref. (*9*).

under the ^{15}N chemical shift interaction with proton decoupling. A moving ^{15}N 180° pulse not only matches the ^{15}N evolution time to the C-H coupling period but also doubles the apparent magnitude of the ^{15}N CSA. The doubling makes the effective strengths of the ^{15}N CSA and C-H coupling comparable, thus leading to enhanced spectral variation with respect to the torsion angle (*9, 23*). Again, to maintain synchronization with sample rotation, the ^{15}N evolution period is placed in a constant time of one rotor cycle. At the end of the ^{15}N evolution, another pair of 90° pulses and a REDOR mixing period convert the coherence C_zN_x into observable ^{13}C magnetization, which is detected during t_2. Absorptive, sign-sensitive spectra in ω_1 are obtained by recording the cosine and sine components of the ^{15}N chemical shift in separate data sets according to the method of Ruben and co-workers (*25*).

Similar to the double- and zero-quantum HNCH technique introduced earlier (*8*), the current experiment gives rise to the sum of two interaction frequencies in the ω_1 dimension. However, this is achieved by separate evolutions of the ^{13}C and ^{15}N antiphase magnetizations rather than the simultaneous evolution of the double- and zero-quantum N-C coherence. The separation of the two evolution periods is necessary since the protons need to be *coupled* to $^{13}C^\alpha$ in order to measure the C-H

couplings but be *decoupled* from ^{15}N for measuring the ^{15}N chemical shift. The advantage of the synchronous evolution can be understood by comparing it with an alternative 3D experiment with two independently incremented evolution periods. Synchronous evolution reduces signal-averaging time considerably, thus making the experiment more applicable to large biomolecules. It also avoids undesirable dispersive sideband lineshapes that could be present in the anisotropic planes of the 3D experiment (*26*).

Alternatively, in-phase magnetizations (C_y, N_y) could be employed in the evolution periods. This would require the use of cross polarization (CP) between the two low-γ nuclei (*27*). Several variable-amplitude spin lock methods should be considered in implementing such a double CP experiment in order to obtain maximum transfer efficiency (*28–30*).

Torsion-angle dependence of the time signal. The pulse sequence modulates the spin density operator during t_1 according to $\cos(\Psi_{CH}(t_1))\exp(i\Psi_N(t_1))$, where $\Psi_\lambda(t_1) = \int_0^{t_1} dt\omega_\lambda(t)$ is the dynamic phase accumulated under the interaction λ. This modulation can be rewritten in terms of the sum and difference of the two phases,

$$\tfrac{1}{2}\left[e^{i(\Psi_N(t_1)+\Psi_{CH}(t_1))} + e^{i(\Psi_N(t_1)-\Psi_{CH}(t_1))}\right]. \qquad [1]$$

where the sum and difference phases

$$\Psi_N(t_1) \pm \Psi_{CH}(t_1) = \int_0^{t_1} dt(\omega_N(t) \pm \omega_{CH}(t)) \qquad [2]$$

contain integrals over the sum and difference frequencies of the chemical shift and dipolar coupling. Such sum and difference frequencies depend on the relative orientation of the ^{15}N chemical shift and C-H interaction tensors. Since the two principal axes systems (PAS) are fixed in the two segments across the torsion axis N-C^α, and neither tensor is uniaxial along this axis, the relative orientation of the two tensors reflects the torsion angle ϕ around this bond. If the orientation of each interaction PAS is expressed by Euler angles $\Omega_\lambda = (\alpha_\lambda, \beta_\lambda, \gamma_\lambda)$, and if the N-$C^\alpha$ bond is chosen as the z-axis of the molecular frame, then $|\gamma_N - \gamma_{CH}|$ corresponds to the torsion angle ϕ, apart from a constant that corresponds to the γ-difference in the $\phi = 0°$ conformation.

In exact analogy to standard MAS theory, it can be shown that the sidebands obtained from the sum and difference frequencies for an isotropic sample are absorptive and positive (*31, 32*), as long as the two evolution periods t_1 are equal in length and start at identical rotor orientations. This is ensured in the pulse sequence by constant-time evolution of the ^{13}C and ^{15}N coherences.

Simulated ^{15}N CSA/C^α-H^α correlation spectra. To demonstrate the sensitivity of the ^{15}N CSA/C^α-H^α spectra to ϕ, we calculated the rotational sideband spectra as a function of ϕ. The spectra are calculated in the time domain by analytical evaluation of Eq. [1] over the course of the evolution period. The N-C dipolar coupling, which is not averaged out during the ^{15}N chemical shift evolution, is also included. Each FID is calculated for one rotor period of 360 μs using a t_1 dwell time of 18 μs. It is replicated many times to produce an apparent acquisition time of 18.4 ms, then exponentially broadened by 150 Hz, and finally Fourier transformed to give the frequency spectrum.

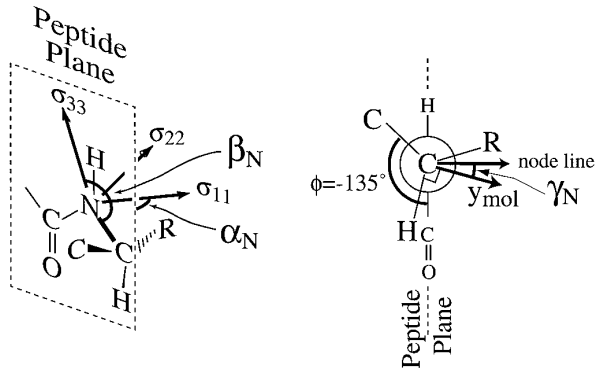

FIG. 2. Orientation of the chemical shift principal axis system of a peptide backbone ^{15}N atom and the Euler angles that rotate the tensor to the molecular frame. The molecular frame is defined by a z-axis along the N-C^α bond and a y-axis (y_{mol}) perpendicular to the N-C^α-H^α plane. β_N is the angle between the σ_{33} axis and the N-C^α bond. α_N is the angle between the σ_{22} axis and the normal to the peptide plane, or equivalently, the angle between the σ_{11} axis and (its projection in) the peptide plane. α_N is found to deviate from 0° by about 25° in NAV. γ_N is the angle between the normal to the peptide plane (the "node line" of the Euler rotation) and the y_{mol}-axis. The ϕ angle shown here is that of NAV and corresponds to an extended β-sheet conformation.

As shown in Fig. 2, the common molecular frame in the simulation is chosen with the z-axis along the N-C^α bond and with the x-axis in the $H^\alpha C^\alpha N$ plane. In this common frame, the Euler angles describing the C-H bond orientation are $\Omega_{CH} = (0°, 109.5°, 0°)$, while those for the ^{15}N chemical shift tensor orientation are $\Omega_N = (\alpha_N, \beta_N, \gamma_N) = (-20°, 137°, 240° - \phi)$. The choice of $\alpha_N = -20°$ is based on a recent report of the ^{15}N shift tensor orientation in Ala-^{15}N-Leu (*13*), where correlation of the N-H coupling, ^1H shift, and ^{15}N shift tensors in a 3D spectrum yielded α_N of 10° to 30°. It differs from a previous result on NAV ($\alpha_N \approx 0$), which was obtained by correlating the N-H dipolar coupling with the ^{15}N tensor (*11*). However, as stated in that paper, the experiment mainly determined the angle between the N-H bond and the σ_{33} axis and could not constrain the orientations of the σ_{11} and σ_{22} axes sufficiently due to the small asymmetry of the tensor. A detailed RMSD analysis shown below in Fig. 8 indicates that $\alpha_N = 0$ is inconsistent with the experimental spectrum of NAV (Fig. 6).

Other simulation parameters include the effective C-H coupling (10.4 kHz), the ^{15}N CSA (−8.51 kHz), the N-C coupling (1.0 kHz), the REDOR mixing time (720 μs), and the spinning

speed (2.778 kHz). These parameters are taken from the experimental spectrum of NAV shown in Fig. 6. The number of crystallites in the powder average is 5000.

Figure 3 exhibits the calculated ^{15}N CSA/C$^{\alpha}$-H$^{\alpha}$ rotational sideband spectra as a function of ϕ. The spectra show significantly asymmetric sideband envelopes with respect to the zero frequency, in marked contrast to the symmetric spectra of the dipolar HNCH experiment. Correspondingly, nearly twice as many independent sidebands are available from these CSA-based spectra, which aids the determination of the best-fit ϕ angle. Pairs of spectra with complementary ϕ angles $\phi_1 + \phi_2 = 120°, -240°$ that cannot be distinguished by pure dipolar correlation (*8*) are displayed side by side. Though similarities still remain, the spectral differences are well visible, especially when ϕ corresponds to the β-sheet conformation ($-160°$ and $-80°$, $-140°$ and $-100°$). The polarity of the spectra reverses between $-20°$ and $-60°$, and between 140° and 180°.

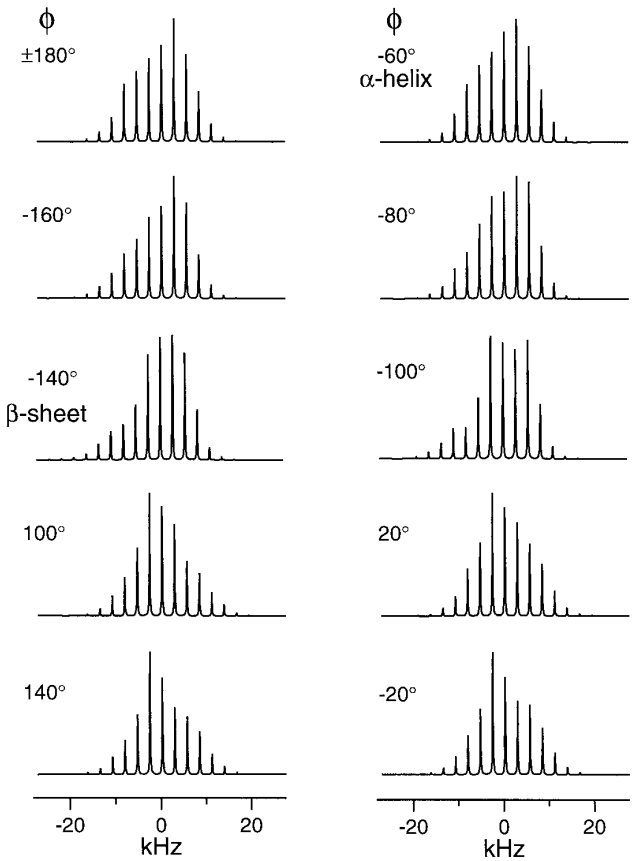

FIG. 3. Calculated ^{15}N CSA/C$^{\alpha}$-H$^{\alpha}$ spectra as a function of the torsion angle ϕ with 20° increments. The spectra are simulated with the following parameters. ^{15}N $\delta_{CSA} = -8512$ Hz (-107 ppm in a 9.4-T magnetic field), $\eta_{CSA} = 0.27$, as determined from the ^{15}N spectra shown below, $\omega_{CH} = 10.4$ kHz according to the DIPSHIFT experiment. The Euler angles rotating the ^{15}N CSA tensor to the N-C$^{\alpha}$ common frame are $(\alpha_N, \beta_N, \gamma_N) = (-20°, 137°, 240° - \phi)$. The corresponding Euler angles for the C-H coupling are (0°, 109.5°, 0°). The spinning speed is $\omega_r/2\pi = 2778$ Hz.

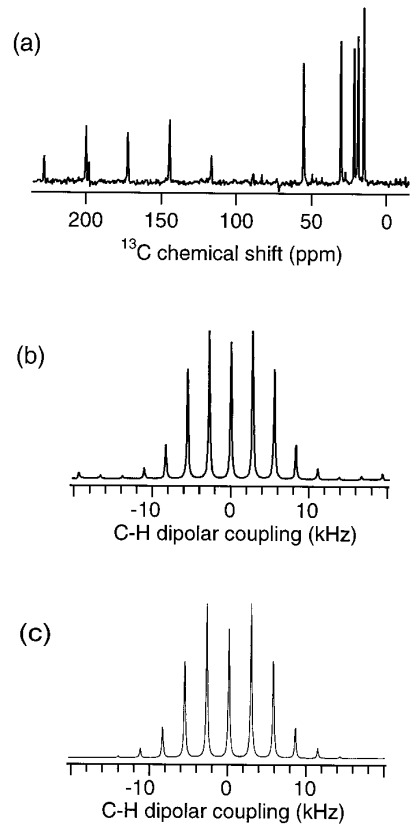

FIG. 4. The ^{13}C-^{1}H DIPSHIFT of NAV. (a) ω_2 spectrum, showing the ^{13}C isotropic shifts. (b) ω_1 cross section of the C$^{\alpha}$ resonance. (c) Corresponding simulation with an effective dipolar coupling of 10.4 kHz.

RESULTS AND DISCUSSIONS

C-H dipolar coupling. The correlation of the ^{15}N CSA and C$^{\alpha}$-H$^{\alpha}$ dipolar coupling requires knowledge of the size and the orientation of these interactions. The size of the C$^{\alpha}$-H$^{\alpha}$ dipolar coupling is scaled from the one-bond coupling constant by the MREV-8 sequence. Since only the product of the rigid-limit coupling strength and the MREV-8 scaling factor is relevant for the current experiment, it is unnecessary to have precise knowledge of each parameter independently. In fact, the one-bond C-H coupling constant is known to be smaller than the theoretical value due to vibrational averaging effects (*33*), and the scaling factor of MREV-8 is cumbersome to measure. Thus, we determined the scaled C-H dipolar couplings using a DIPSHIFT experiment in which the C-H couplings are separated according to the ^{13}C chemical shift (*34*). The MREV-8 parameters and the t_1 dwell time are set to be the same as in the torsion angle experiment. Figure 4a shows the ω_2 projection of the 2D spectrum, which exhibits the expected five aliphatic resonances and the carbonyl sideband manifold. Taking the ω_1 spectrum of the C$^{\alpha}$ resonance at 55 ppm (Fig. 4b), we observe a symmetric rotational sideband pattern, whose intensities are fit to yield a dipolar coupling strength of 10.4 $\pm$ 0.5 kHz (Fig. 4c).

^{15}N chemical shift anisotropy. The principal values of the ^{15}N chemical shift tensor exhibit non-negligible variations among different peptides. Fortunately, they can be measured conveniently by one-dimensional (1D) CP experiments in the case of a single ^{15}N site or by two-dimensional (2D) anisotropic-isotropic chemical shift separation techniques (*35–38*) in the case of multiple ^{15}N sites. The asymmetry parameter (η) of the amide ^{15}N chemical shift tensor in peptides varies from as low as <0.1 (mainly glycine) to as high as >0.35 (*14, 16, 17, 19*).

The ^{15}N chemical shift anisotropy of NAV was measured by a static ^{15}N CP experiment. The powder pattern (Fig. 5a) is characterized by an anisotropy of $\delta = \sigma_{33} - \sigma_{iso} = 106$ ppm and an asymmetry parameter of $\eta = 0.27$. In the 9.4-T magnetic field used, this CSA (4.3 kHz) amounts to less than half of the one-bond C-H dipolar coupling constant (ca. 11 kHz). This justifies the doubling procedure used in the pulse sequence (*9*), since the maximal spectral variation with the torsion angle occurs when the two interaction strengths are comparable.

To ensure that the CSA-doubled ^{15}N spectrum obtained under MAS is consistent with the static spectrum, we performed a control experiment using the pulse sequence of Fig. 1 but without CH dipolar evolution under MREV-8 decoupling. This yields a pure ^{15}N CSA spectrum without the C-H dipolar coupling. As shown in Fig. 5c, the ^{15}N sideband spectrum indicates that the width of the shift anisotropy is indeed doubled with respect to the powder pattern. Further, the sense of asymmetry of the sideband spectrum is the same as the static spectrum under the phase cycles for the ^{15}N 180° pulse and for the receiver. Knowledge of the spectral asymmetry is important for simulating the torsion angle spectra with the correct sign. A best-fit simulation of the pure ^{15}N CSA sideband spectrum is shown in Fig. 5d. In this simulation, the unrefocused N-C dipolar coupling with a double magnitude (2 kHz) is taken into account.

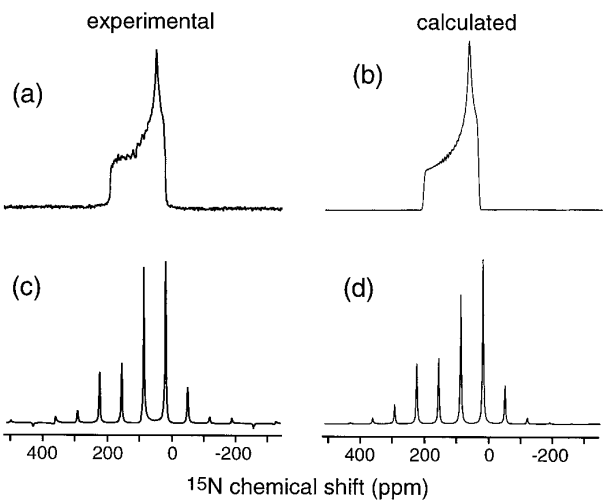

FIG. 5. The ^{15}N chemical shift spectra of NAV. (a) Powder spectrum obtained without sample rotation. A total of 928 scans were averaged. (b) Simulation of the static spectra with $\delta = 106$ ppm and $\eta = 0.27$. (c) CSA-doubled MAS spectrum, taken at $\omega_r/2\pi = 2778$ Hz and with the 2D pulse sequence in Fig. 1b but without the C-H coupling evolution. (d) Simulation of the MAS spectra with $\delta = 212$ ppm.

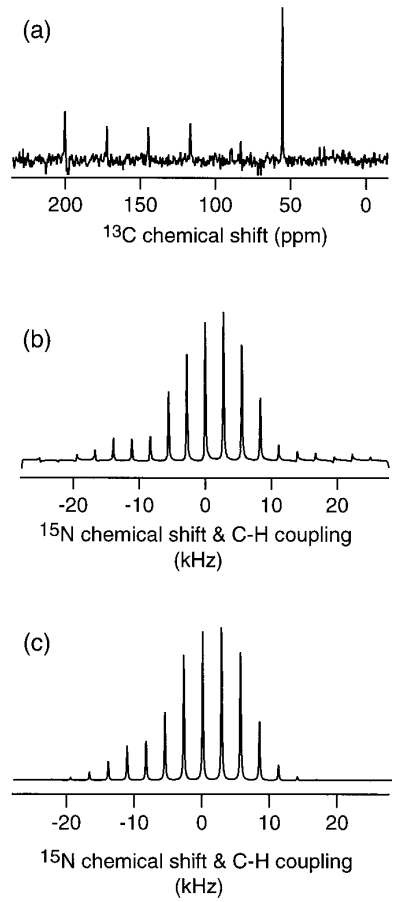

FIG. 6. The ^{15}N CSA/C$^{\alpha}$-H$^{\alpha}$ correlation spectrum. (a) ω_2 dimension at $t_1 = 0$, showing the selection of C$^{\alpha}$ resonance and acetyl carbonyl resonance by the REDOR mixing period. (b) ω_1 cross section of C$^{\alpha}$, reflecting the mutual orientation of the ^{15}N CSA tensor and the C$^{\alpha}$-H$^{\alpha}$ dipolar tensor. (c) Best-fit simulation with $\phi = -140°$. The azimuthal angle of the N-C$^{\alpha}$ bond in the ^{15}N chemical shift principal-axes system is $\alpha = -25°$.

^{15}N CSA/C$^{\alpha}$-H$^{\alpha}$ correlation spectra. The ^{15}N CSA/C$^{\alpha}$-H$^{\alpha}$ correlation spectrum of NAV is shown in Fig. 6. In the ω_2 dimension (Fig. 6a), only the C$^{\alpha}$ and the acetyl carbonyl resonances survive due to the relatively short N-C transfer time used. The ω_1 cross section of the C$^{\alpha}$ peak (Fig. 6b) displays an asymmetric spectral envelope with much higher intensities in the first three orders of sidebands than those in Fig. 5c due to the contribution of the C-H coupling. The best-fit simulation of the spectrum (Fig. 6c), obtained with $\alpha_N = -25°$, yields $\phi = -140°$, which agrees well with the x-ray crystal structure of $\phi = -136.5°$ (*40*). The choice of α_N in the best-fit simulation is discussed in more detail below.

Angular resolution. In order to quantify the angular resolution of the ^{15}N CSA/C$^{\alpha}$-H$^{\alpha}$ correlation technique, i.e., the

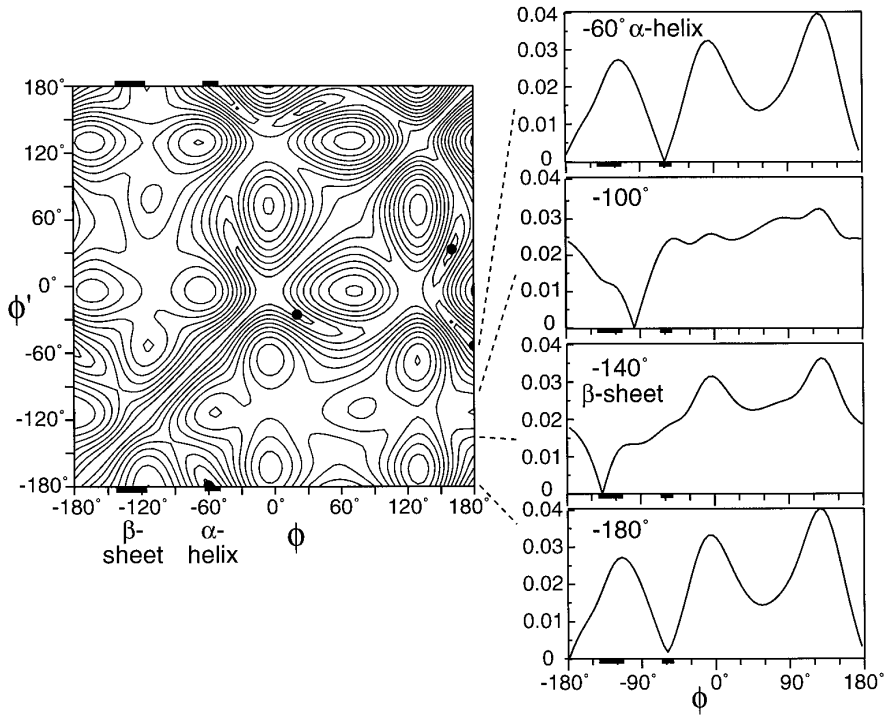

FIG. 7. The 2D RMSD contour plot for quantifying the angular resolution of the ^{15}N CSA/C$^{\alpha}$-H$^{\alpha}$ technique. The ^{15}N CSA/C$^{\alpha}$-H$^{\alpha}$ spectra were calculated with $\alpha_N = -25°$ and as a function of ϕ at 5° increments, giving 72^2 points in the 2D plot. The contour heights correspond to the difference between spectra for the pair of ϕ angles defined by the *x*- and *y*-position. Three points of exactly vanishing RMSD in the lower right half of the plot are indicated by dots. Regions of β-sheet and α-helix conformations are emphasized by bars. Several cross sections through the 2D plot at the indicated ϕ values are shown on the right.

degree of difference between spectra of different torsion angles, we calculated the root-mean-square deviations (RMSD) between pairs of simulated spectra. As described previously (*9*), the RMSD is defined as

$$\mathrm{RMSD}(\phi, \phi') = \{\sum_{i=1}^{N} [S_i(\phi) - S_i(\phi')]^2/N\}^{1/2}, \qquad [3]$$

where $S_i(\phi)$ is the normalized intensity of the *i*th sideband, out of $N = 14$ sidebands in a spectrum of torsion angle ϕ. The result for 72^2 pairs of ϕ-angle spectra, calculated in increments of 5° for $-180° \le \phi \le 180°$ and with $\alpha_N = -25°$, is shown in a 2D RMSD contour plot (Fig. 7) as a function of ϕ and ϕ'. Each spectrum is averaged over 648,000 crystallite orientations. The intensities of the contour lines reflect the spectral variation due to the ϕ angle. The higher the contour intensity, the larger the spectral difference. Since RMSD(ϕ, ϕ) = 0, the contour intensity along the main diagonal of the 2D is zero. Near the diagonal between about $-180°$ and $-15°$, the contour lines are more densely spaced, indicating significant spectral changes, or high angular resolution. Several cross sections through the 2D contour plot are also shown. In these cross sections, the relative widths of the global minima at a fixed RMSD value indicate the relative angular resolution. For example, the angular resolution at $\phi = -140°$, which corresponds to the β-sheet structure, is better than that around $\phi = -60°$, which corresponds to the α-helix conformation. It can also be seen that the traces for $-100°$ and $-140°$, which are identical in the pure dipolar HNCH correlation experiment, are clearly different here. This shows that even a relatively small deviation of the ^{15}N σ_{11} axis from the peptide plane ($\alpha_N = -25°$) can effectively remove the spectral degeneracy around $\phi = -120°$. The similarity between the $-60°$ and the $-180°$ traces results from one of the three discrete degeneracies in the full 2D contour plot. Finally, in both the $-60°$ and the $-140°$ cross sections, the RMSD values differ greatly between $\phi = -140°$ and $\phi = -60°$, indicating that the β-sheet conformation and the α-helix structure can be clearly distinguished.

Requirements for full-range ϕ determination. In our previous HNCH correlation experiments, the spectra for pairs of ϕ angles centered around $-120°$ and $+60°$ are identical. These degeneracies occur because the relative orientation of the unique axes of two dipolar tensors is characterized by only one parameter, the angle between the axes. The correlation involving the non-uniaxial ^{15}N chemical shift interaction is less prone to such degeneracies, since the relative tensor orientation depends on two angles, which are the polar coordinates of the C$^{\alpha}$-H$^{\alpha}$ dipolar axis in the ^{15}N chemical shift principal axes system. As discussed previously (*1*), systematic degeneracies occur only if a principal axis of either tensor is perpendicular

to the torsion bond. For a uniaxial interaction, one of the degenerate principal axes always fulfills this condition. For the peptide ^{15}N chemical shift, one principal axis would be perpendicular to the N-C$^{\alpha}$ bond if the azimuthal angle α_N of that bond in the chemical shift PAS is 0°, 90°, 180°, or 270°. The additional case of the polar angle $\beta_N = 90°$ can be safely excluded based on the literature data for the ^{15}N chemical shift tensor orientation, where $\beta_N \approx 140°$ (*13, 14*). For $\alpha_N = 0°$, $\pm 90°$, or 180°, the degeneracy is the same as in the pure dipolar HNCH experiments. It is centered around $\phi = -120°$ and $+60°$, so that, for instance, the spectra for $\phi = -140°$ and $-100°$ are identical. For $\alpha_N \neq 0$ and the given orientation of the ^{15}N CSA tensor, only three discrete degeneracies occur. They can be identified as isolated minima at the zero level in Fig. 7.

While the angle β_N between the N-C$^{\alpha}$ bond and the σ_{33} axis of the ^{15}N chemical shift tensor does not vary significantly among different amino acid residues, α_N values between 0° and 20° have been estimated from correlation of the ^{15}N chemical shift anisotropy with a segment-fixed dipolar coupling (*13, 16*). If the peptide group were strictly planar and the chemical shift only reflected the local symmetry, then $\alpha_N = 0°$, 180° or $\pm 90°$ would be required. However, the peptide group is not completely planar in NAV according to the x-ray crystal structure (*39*). In addition, long-range γ-gauche effects in β-branched amino acid sidechains can shift the ^{15}N tensor orientation further away from $\alpha_N = 0$ (*40*).

We investigated the effect of the angle α_N on the determination of the best-fit ϕ torsion angle by calculating the RMSD between the experimental and the simulated torsion angle spectra as a function of ϕ for several different values of α_N (Fig. 8). As expected, the traces for $\alpha_N = 0°$ and 90° exhibit the undesired symmetry around $\phi = -120°$ and $\phi = 60°$, which is the same as that observed in the HNCH experiment. The orientation of $\alpha_N = 0°$ can be safely excluded because the fits indicate relatively large RMSD values, while $\alpha_N = -90°$ is completely inconsistent with the literature. For α_N between $-20°$ and $-90°$, a pronounced minimum is observed near $\phi = -140°$, which is close to the value found in the x-ray crystal structure ($\phi = -136.5°$). The exact position of the RMSD minima for α_N between $-25°$ and $-90°$ are not very different. This can be understood because changing α_N with fixed β_N leaves the σ_{33} axis unaffected but changes the orientations of the σ_{22} and σ_{11} principal axes. Since these two principal values are relatively similar, the resulting spectral variations are small. However, we point out that for α_N values of the opposite sign the minimum appears at $\phi = -100°$. Thus, a full-range determination of ϕ requires knowledge of the sign of α_N. For NAV, given the x-ray crystal structure and the small absolute values of α_N in the literature, the sign of α_N must be negative and its most probable value is $-25°$. Note that other NMR techniques that correlate the ^{15}N CSA tensor with the N-C′, N-C$^{\alpha}$, or N-H dipolar couplings cannot yield the sign of α_N.

The observed insensitivity of the best-fit ϕ torsion to α_N within the relevant angular range means that it is possible to determine ϕ even without precise knowledge of α_N. Due to the significant difference in the N-H dipolar and ^{15}N chemical-shift tensor orientations, their correlation with the C-H dipolar coupling responds differently to ϕ-angle changes. This fact, combined with the asymmetry of the CSA/dipolar sideband spectrum, makes the ^{15}N CSA/C$^{\alpha}$-H$^{\alpha}$ experiment useful for corroborating the result of the HNCH experiment and increasing its precision in regions where the ϕ resolution of the latter is low.

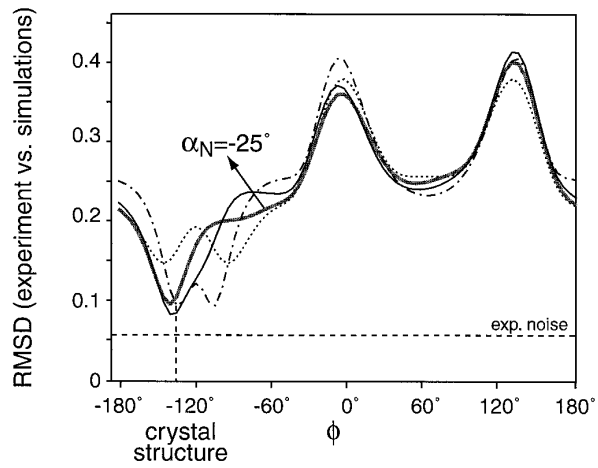

FIG. 8. RMSD between the experimental and the simulated spectra as a function of ϕ and parameterized by α_N, which is the angle between the σ_{22} axis of the ^{15}N CSA tensor and the normal to the peptide plane. The RMSD values are reported as fractions of the total experimental spectral intensity. Four different curves are plotted, corresponding to $\alpha_N = 0°$ (dotted line), -25 (thick solid line), $-50°$ (thin solid line), and $-90°$ (dashed line). 72 spectra with 5° ϕ-angle increments are calculated for each RMSD curve. The experimental rms noise, which is calculated based on the intensities of six noise sidebands at the two edges of the experimental spectrum, is shown as a dashed horizontal line at 6%. The fact that this noise level is smaller than the rmsd between the experiment and the best fit simulation suggests that systematic error, in addition to random error, contributes to the experimental uncertainty.

CONCLUSIONS

We demonstrated a dipolar-chemical shift correlation technique for determining the peptide torsion angle ϕ potentially over the full range of 360°. The technique breaks the spectral degeneracy in previous HNCH correlation experiments by employing the asymmetric chemical shift interaction of the peptide backbone ^{15}N. Correlation of the ^{15}N CSA and C$^{\alpha}$-H$^{\alpha}$ coupling interaction yields the relative orientation of the two tensors and hence the H^{N}-N-C$^{\alpha}$-H$^{\alpha}$ torsion angle. Doubling of the magnitude of the ^{15}N CSA relative to the C$^{\alpha}$-H$^{\alpha}$ dipolar coupling achieves an angular resolution of better than $\pm 10°$ in the biologically interesting β-sheet region, as estimated by an RMSD analysis. Because of the asymmetry of the ^{15}N-CSA/C$^{\alpha}$-H$^{\alpha}$ spectrum, the number of independent conformation-sensitive sidebands is doubled compared to the pure dipolar

HNCH experiment. If the orientation of the σ_{11} axis of the ^{15}N chemical shift principal-axes system is exactly known, then the twofold degeneracy of the ϕ angle is removed and the torsion angle can be determined unambiguously in the full 360° range. Even if the orientation of the σ_{11} axis is not known, the best-fit procedure still provides a good estimate of ϕ, but with a twofold degeneracy. This ^{15}N CSA/C^{α}-H^{α} experiment should be used in conjunction with the HNCH experiment to increase the angular precision of the ϕ determination. The experiment, demonstrated here on ^{15}N-enriched but ^{13}C-natural abundance NAV, has sufficient sensitivity to be applied to larger ^{13}C- and ^{15}N-labeled peptides and proteins for the simultaneous determination of many ϕ torsion angles.

EXPERIMENTAL

Powder NAV was obtained from Cambridge Isotope Laboratories, Inc. (Andover, MA) and was recrystallized in aqueous solution. The spectra were measured on a homebuilt spectrometer operating at 397.8 MHz for ^1H, 100.0 MHz for ^{13}C, and 40.3 MHz for ^{15}N nuclei. A homebuilt triple resonance probe with a transmission line design and equipped with a 4-mm Chemagnetics (Fort Collins, CO) MAS spinning module was used. Proton RF fields of about 100 kHz were used for excitation and CW decoupling. The ^1H 90° pulse length for MREV-8 multiple-pulse decoupling was 3 μs. Semi-windowless MREV-8 was used and incremented in half cycles of 18 μs during the C-H evolution period. The spinning speed was 2778 Hz and was controlled by a Doty (Columbia, SC) spinning speed controller to within 2 Hz.

ACKNOWLEDGMENTS

This research at MIT was supported by the National Institute of Health (GM-23403, GM-23289, and RR-00995). M. Hong was supported by a NIH postdoctoral fellowship (GM-18870). The authors thank Prof. K. Schmidt-Rohr for helpful discussions.

REFERENCES

1. K. Schmidt-Rohr, A double-quantum solid-state NMR technique for determining torsion angles in polymers, *Macromolecules* **29,** 3975–3981 (1996).
2. K. Schmidt-Rohr, Torsion angle determination in solid 13C-labeled amino acids and peptides by separated-local-field double-quantum NMR, *J. Am. Chem. Soc.* **118,** 7601–7603 (1996).
3. R. Tycko and D. Weliky, Investigation of molecular structure in solids by two-dimensional NMR exchange spectroscopy with magic angle spinning, *J. Chem. Phys.* **105** (1996).
4. J. Kummerlen, J. D. vanBeek, F. Vollrath, and B. Meier, Local structure in spider dragline silk investigated by two-dimensional spin-diffusion nuclear magnetic resonance, *Macromolecules* **29,** 2920–2928 (1996).
5. X. Feng, Y. K. Lee, D. Sandstroem, M. Eden, H. Maisel, A. Sebald, and M. H. Levitt, Direct determination of a molecular torsional angle by solid-state NMR, *Chem. Phys. Lett.* **257,** 314–320 (1996).
6. D. M. Gregory, M. A. Mehta, J. C. Shields, and G. P. Drobny, Determination of local structure in solid nucleic acids using double quantum NMR spectroscopy, *J. Chem. Phys.* **107,** 28–42 (1997).
7. Y. Ishii, T. Terao, and M. Kainosho, Relayed anisotropy correlation NMR: Determination of dihedral angles in solids, *Chem. Phys. Lett.* **256,** 133–140 (1996).
8. M. Hong, J. D. Gross, and R. G. Griffin, Site-resolved determination of peptide torsion angle phi from the relative orientations of backbone N-H and C-H bonds by solid-state NMR, *J. Phys. Chem. B* **101,** 5869–5874 (1997).
9. M. Hong, J. D. Gross, C. M. Rienstra, R. G. Griffin, K. K. Kumashiro, and K. Schmidt-Rohr, Coupling amplification in 2D MAS NMR and its application to torsion angle determination in peptides, *J. Magn. Reson.,* in press.
10. P. R. Costa, J. D. Gross, M. Hong, and R. G. Griffin, Solid-state NMR measurement of ψ in peptides: A NCCN 2Q-heteronuclear local field experiment, *Chem. Phys. Lett.* **280,** 95–103 (1997).
11. J. E. Roberts, G. S. Harbison, M. G. Munowitz, J. Herzfeld, and R. G. Griffin, Measurement of heteronuclear bond distances in polycrystalline solids by solid-state NMR techniques, *J. Am. Chem. Soc.* **109,** 4163–4169 (1987).
12. A. C. Kolbert and R. G. Griffin, Two-dimensional spin-echo dipolar-sideband enhancement in magic-angle-spinning NMR, *J. Magn. Reson.* **93,** 242–255 (1991).
13. C. H. Wu, A. Ramamoorthy, L. M. Gierasch, and S. J. Opella, Simultaneous characterization of the amide 1H chemical shift, 1H-15N dipolar, and 15N chemical shift interaction tensors in a peptide bond by three-dimensional solid-state NMR, *J. Am. Chem. Soc.* **117,** 6148–6149 (1995).
14. T. G. Oas, C. J. Hartzell, F. W. Dahlquist, and G. P. Drobny, The amide 15N chemical shift tensors of four peptides determined from 13C dipole-coupled chemical shift powder patterns, *J. Am. Chem. Soc.* **109,** 5962–5966 (1987).
15. C. J. Hartzell, T. K. Pratum, and G. Drobny, Mutual orientation of three magnetic tensors in a polycrystalline dipeptide by dipole-modulated 15N chemical shift spectroscopy, *J. Chem. Phys.* **87,** 4324–4331 (1987).
16. C. J. Hartzell, M. Whitfeld, T. G. Oas, and G. P. Drobny, Determination of the 15N and 13C chemical shift tensors of L-[13C]alanyl-L-[15N]alanine from the dipole-coupled powder patterns, *J. Am. Chem. Soc.* **109,** 5966–5969 (1987).
17. W. Mai, W. Hu, C. Wang, and T. A. Cross, Orientational constraints as 3D structural constraints from CSA: The polypeptide backbone of gramicidine A in a lipid bilayer, *Protein Sci.* **2,** 532–542 (1993).
18. G. S. Harbison, L. W. Jelinski, R. E. Stark, D. A. Torchia, J. Herzfeld, and R. G. Griffin, 15N chemical shift and 15N-13C dipolar tensors for the peptide bond in [1-13C] glycyl [15N] glycine hydrochloride monohydrate, *J. Magn. Reson.* **60,** 79–82 (1984).
19. A. Shoji, S. Ando, S. Kuroki, I. Ando, and G. A. Webb, Structural studies of peptides and polypeptides in the solid state by ^{15}N NMR, *Ann. Rep. NMR Spectrosc.* **26,** 55–98 (1993).
20. M. Hong, A. Pines, and S. Caldarelli, Measurement and assignment of long-range C–H dipolar couplings in liquid crystals by two-dimensional NMR spectroscopy, *J. Phys. Chem.* **100,** 14,815–14,822 (1996).
21. T. Gullion and J. Schaefer, Rotational echo double resonance NMR, *J. Magn. Reson.* **81,** 196–200 (1989).
22. W.-K. Rhim, D. D. Elleman, and R. W. Vaughan, Analysis of multiple-pulse NMR in solids, *J. Chem. Phys.* **59,** 3740–3749 (1973).
23. T. Gullion and J. Schaefer, Detection of weak heteronuclear dipolar coupling by rotational-echo double-resonance nuclear magnetic

resonance, *in* "Advances in Magn. Reson." (W. S. Warren, Ed.), pp. 57–83, Academic Press, San Diego (1989).

24. D. J. States, R. A. Haberkorn, and D. J. Ruben, A 2D NOE experiment with pure absorption phase in four quadrants, *J. Magn. Reson.* **48,** 286–292 (1982).

25. M. G. Munowitz and R. G. Griffin, Two-dimensional NMR in rotating solids: An analysis of line shapes in chemical shift-dipolar spectra, *J. Chem. Phys.* **76,** 2848–2858 (1982).

26. J. Schaefer, E. O. Stejskal, J. R. Garbow, and R. A. McKay, Quantitative determination of the concentration of 13C-15N chemical bonds by double cross-polarization NMR, *J. Magn. Reson.* **59,** 150–156 (1984).

27. M. Baldus, D. G. Geurts, S. Hediger, and B. H. Meier, Efficient 15N-13C polarization transfer by adiabatic-passage Hartmann–Hahn cross polarization, *J. Magn. Reson. A* **118,** 140–144 (1996).

28. S. Hediger, B. H. Meier, N. D. Kurur, G. Bodenhausen, and R. R. Ernst, NMR cross polarization by adiabatic passage through the Hartman–Hahn condition (APHH), *Chem. Phys. Lett.* **223,** 283–288 (1994).

29. S. Hediger, V. H. Meier, and R. R. Ernst, Cross polarization under fast magic angle spinning using amplitude-modulated spin-lock sequences, *Chem. Phys. Lett.* **213,** 627–635 (1993).

30. A. C. Kolbert and S. L. Gann, Variable-effective-field cross polarization. An approach to broadband Hartmann–Hahn matching in MAS NMR, *Chem. Phys. Lett.* **224,** 86–90 (1994).

31. J. Herzfeld and A. E. Berger, Sideband intensities in NMR spectra of samples spinning at the magic angle, *J. Chem. Phys.* **73,** 6021 (1980).

32. M. H. Levitt, Why do spinning sidebands have the same phase? *J. Magn. Reson.* **82,** 427–433 (1989).

33. E. R. Henry and A. Szabo, Influence of vibrational motion on solid state line shapes and NMR relaxation, *J. Chem. Phys.* **82,** 4753–4761 (1985).

34. M. G. Munowitz, R. G. Griffin, G. Bodenhausen, and T. H. Huang, Two-dimensional rotational spin-echo NMR in solids: Correlation of chemical shift and dipolar interactions, *J. Am. Chem. Soc.* **103,** 2529–2533 (1981).

35. T. Terao, T. Fujii, T. Onodera, and A. Saika, Switching-angle sample-spinning NMR spectroscopy for powder-pattern- resolved 2D spectra: Measurement of 13C chemical-shift anisotropies in powdered 3,4-dimethoxybenzaldehyde, *Chem. Phys. Lett.* **107,** 145–148 (1984).

36. R. Tycko, G. Dabbagh, and P. Mirau, Determination of chemical-shift-anisotropy lineshapes in a two-dimensional magic-angle-spinning NMR experiment, *J. Magn. Reson.* **85,** 265–274 (1989).

37. L. Frydman, G. C. Chingas, Y. K. Lee, P. J. Grandinetti, M. A. Eastman, G. A. Barrall, and A. Pines, Variable-angle correlation spectroscopy in solid-state nuclear magnetic resonance, *J. Chem. Phys.* **97,** 4800 (1992).

38. K. Schmidt-Rohr, M. Wilhelm, A. Johansson, and H. W. Spiess, Determination of chemical-shift tensor in methylene groups by separated-local-field NMR, *Magn. Reson. Chem.* **31,** 352–356 (1993).

39. P. J. Carroll, P. L. Stewart, and S. J. Opella, Structures of two model peptides: N-acetyl-D,L-valine and N-acetyl-L-valyl-L-leucine, *Acta Cryst. C* **46,** 243–246 (1990).

40. H. Le and E. Oldfield, Correlation between 15N NMR chemical shifts in proteins and secondary structure, *J. Biomol. NMR* **4,** 341–348 (1994).